

Formation of the First Planetesimals via the Streaming Instability in Globally Turbulent Protoplanetary Disks?

PAUL R. ESTRADA¹ AND ORKAN M. UMURHAN^{1,2,3,4,*}

¹*Space Sciences Division, Planetary Systems Branch, NASA Ames Research Center, Mail Stop 245-3, Moffett Field, CA 94035, USA*

²*SETI Institute, 389 Bernardo Way, Mountain View, CA 94043, U.S.A.*

³*Cornell Center for Astrophysics and Planetary Sciences, Cornell University, Ithaca, NY 14853, USA*

⁴*Department of Earth & Planetary Sciences, University of California Berkeley, Berkeley, CA 94720, USA[†]*

(Received February 8, 2023)

Submitted to *Astrophysical Journal*

ABSTRACT

Using self-consistent models of turbulent particle growth in an evolving protoplanetary nebula of solar composition we find that recently proposed local metallicity and Stokes number criteria necessary for the streaming instability to generate gravitationally bound particle overdensities are generally not approached anywhere in the disk during the first million years, an epoch in which meteoritic and observational evidence strongly suggests that the formation of the first planetesimals and perhaps giant planet core accretion is already occurring.

Keywords: Protoplanetary disks

1. INTRODUCTION

Understanding how the first planetesimals were made constitutes perhaps the single most critical linchpin in deciphering the history of planet formation in the solar nebula and beyond. In addition to providing the fundamental building blocks of planetary nuclei envisaged in the core accretion model, clarifying the means by which planetesimals formed should go toward also explaining the extensive chemical and lithological mixing that took place in the early solar disk as evidenced by the meteorite record (e.g., Zolensky et al. 2006; Krot et al. 2009; Joswiak et al. 2012; Kita et al. 2013; Kruijer et al. 2017; Zanda et al. 2018; Marrocchi et al. 2019; Simon et al. 2019).

In this regard, a commonly held view is that planet formation proceeded differently before and after the formation of Jupiter’s core (Nanne et al. 2019; Jacquet et al. 2019). The general perception is that the emer-

gence of the first planetary cores hastens the formation of gravitationally bound planetary structures throughout the disk: that is, a sufficiently massive perturbing body in the form of a giant planet core (putatively in the 10–20 M_{\oplus} range) helps to drive tidal torques within the disk gas that lead to the formation of gaps (e.g. Lin & Papaloizou 1979; D’Angelo et al. 2003; Paardekooper & Johansen 2018), which in turn aid in the trapping of particles at gap edges (e.g., Paardekooper & Mellema 2006; Rice et al. 2006; Desch et al. 2018; Drazkowska et al. 2019). Moreover, the planetary core, embedded in the ambient disk gas, can benefit from an enhanced solids capture rate through the process of pebble accretion (e.g., Ormel & Klahr 2010; Lambrechts & Johansen 2012; Chambers 2014), in which particle-gas drag helps to focus particles onto a growing core. Yet, assembling these cores relies on prior formation of planetesimals.

Interpretations of the meteorite record suggest that the first planetesimals – *i.e.*, the array of 40 – 100 km scale gravitationally bound mass bodies that presumably went into building planetary cores – were formed as early as ~ 0.5 Ma (millions of years) and as late as ~ 3 – 4 Ma after CAIs (Kita & Ushikubo 2012; Connelly et al. 2012; Schrader et al. 2017; Kruijer et al. 2017). Furthermore, the combination of the above-mentioned

Corresponding author: Paul R. Estrada
paul.r.estrada@nasa.gov

* New Horizons Science Team, Co-Investigator

[†] Lecturer 2022-2024 academic years.

chemical and lithological mixing as well as observations of line-broadening in protoplanetary disks (e.g., Teague et al. 2016; Flaherty et al. 2017, 2018; Dullemond et al. 2018, “pp-disk” hereafter) suggest that the early solar nebula was turbulent; indeed, it is increasingly thought that the early stages of evolution of pp-disks are at least weakly-to-moderately turbulent in the regions where particle growth is of the greatest interest ($\lesssim 100$ au, see e.g., reviews by Turner et al. 2014; Lyra & Umurhan 2019; Lesur et al. 2022).

However, particle growth by sticking (typically mm-cm sized for compact pebbles) in pp-disk gas flows encounters growth “barriers” and loss to the central star via radial drift before planetesimals can ever form (see Estrada et al. 2016, and references therein). Fractal, porous aggregates can survive longer in the pp-disk, but under the same nebula conditions eventually they too suffer the same fate as their compact counterparts (Estrada et al. 2022, hereafter E+22). Thus, it has been argued that some mechanism must come into play that collects these growth-frustrated particles into gravitationally bound multi-km sized structures – objects that are “born big” (Morbidelli et al. 2009).

Three mechanisms that could help “leap-frog” across these growth barriers have been cited in the recently released Planetary Science Decadal Survey (National Academies of Sciences, Engineering, and Medicine 2022), which include particle trapping by large scale coherent gaseous vortices (e.g. Raettig et al. 2021, and references therein), and turbulent concentration (e.g. Hartlep & Cuzzi 2020, and references therein). The third and current leading candidate mechanism is the Streaming Instability (SI, hereafter), in which the relative velocity between a pressure-free particle component and a weakly pressure-supported rotating gaseous fluid brings about a gas-drag mediated momentum exchange resonance that leads to high densities in the particle field (Youdin & Goodman 2005; Squire & Hopkins 2018a,b; Lesur et al. 2022). High resolution shearing box simulations under certain conditions predict the SI leads to the efficient formation of a resolved distribution of self-gravitating particle overdensities (e.g., Simon et al. 2017) with resulting rotational profile statistics that appear consistent with the angular momentum distribution observed in the cold-classical Kuiper Belt Object (KBO) population (Nesvorný et al. 2019).

Several studies have examined the question of under what local conditions does the SI operate efficiently to produce gravitationally bound overdensities (Carrera et al. 2015; Yang et al. 2017; Li & Youdin 2021, hereafter C+15, Y+19, LY21, respectively). These studies addressed this matter using the results of direct nu-

merical simulations of shearing box calculations of globally laminar disks covering a range of values in the disk metallicity Z and particle Stokes number St . In these simulations, any turbulence α is *self-generated* in the midplane-settled particle layer with its magnitude dependent on the choice of Z and St .

It is generally reported that the occurrence of strong overdensities by the SI needs the ratio of the midplane solids-to-gas mass density ϵ to hover around or greatly exceed unity. For a range in Stokes numbers ($0.001 < St < 1$) this condition appears to require that at the very minimum Z exceed 0.015. Recently LY21 report from their globally laminar models that the minimum Z needed for occurrence drops to as low as 0.005 for $St > 0.1$. However, LY21 also suggest that the minimum Z ought to increase with and when including external sources of α as well after accounting for model turbulence calculations reported in Gole et al. (2020).

Whether the efficient operation of the SI can be attained in realistic models of the early solar nebula has not yet been established. There are conflicting indications as to whether or not the SI is effective or even viable in disks experiencing global turbulence (Gole et al. 2020; Chen & Lin 2020; Schäfer et al. 2020; Umurhan et al. 2020; Schäfer & Johansen 2022, the last two of these hereafter U+20 and SJ22, respectively) with turbulent intensities $10^{-5} < \alpha < 10^{-3}$ (Lyra & Umurhan 2019; Lesur et al. 2022), strongly depending upon the thermal cooling time (e.g., Richard et al. 2016; Manger et al. 2021). Indeed, even in the laminar case, the settling dust layer generated α is large enough to thwart the SI for $St \mathcal{O}(0.01)$: the recent high resolution simulation of Carrera & Simon (2022) to model the action of the SI in a globally laminar model shows that while midplane settled mm grain-sized dust layers become turbulent at the level of $\alpha \sim 6 \times 10^{-5}$, they do not lead to appreciable overdensities even though the local Z (≈ 0.03) and St (≈ 0.015) conditions of the simulations are expected to be strongly SI active based on the above cited occurrence studies (C+15; Y+17; LY21). Preliminary models of the results of global disk evolution within the first Ma with turbulent particle growth suggest that the conditions for the efficient operation of the SI are not met according to the analytical theories of the SI subject to turbulence (U+20; Chen & Lin 2020) mainly because when the St of the particles or aggregates grow to large enough values, it comes at the expense of a corresponding decrease in the local values of the metallicity due to rapid radial drift (E+22; Estrada & Cuzzi 2022).

The purpose of this study is to ask the question: *Are the conditions under which the SI can produce gravitationally bound particle overdensities actually met in the*

first million years of evolution of globally turbulent protoplanetary nebulae, an epoch in which evidence strongly suggests the first planetesimals formed? In Section 2 we briefly review the state of the science regarding SI, and discuss the so called SI occurrence diagrams. In Section 3 we introduce the global nebula evolution models we use in this work. In Section 4, we discuss the results of our analyses and in Section 5 we summarize our main conclusions.

2. SI OCCURRENCE, A REVIEW

The SI is initiated when a relative stream occurs between the particle phase and the gas. There are several instances of such relative streaming configurations, but the most common setting is when there is a global radial gas pressure gradient which induces the gas to orbit the star slower than the particles. This situation leads to momentum exchange between the two phases causing particles to steadily spiral inward, and the gas outward (e.g., the steady solutions of Nakagawa et al. 1986). The strength of this relative flow is governed by the Stokes number defined in the Epstein regime (where the particle size a is smaller than the gas molecular mean free path) as

$$\text{St} = \frac{3m_p}{4\rho cA} \Omega = \frac{\rho_p a}{\rho c} \Omega, \quad (1)$$

with the second equality corresponding to compact spherical particles where the particle mass-to-cross-sectional-area ratio $(3/4)m_p/A$ reduces to $\rho_p a$. Here, ρ_p is the compact particle internal density, c is the gas sound speed, ρ is the gas density, and Ω is the local disk rotation rate. As this relative flow state takes root, an instability-inducing resonance occurs between the particles and gas when the relative stream velocity matches the wave velocity of an inertial wave in the gaseous component (Squire & Hopkins 2018a). The strength of the SI is sensitive to the midplane solids-to-gas mass density ratio $\epsilon = \rho_{\text{solids}}/\rho$, and it is generally considered to be most explosive when $\epsilon \gtrsim 1$ (e.g., Youdin & Goodman 2005, U+20).

In this scenario, the key ingredient for the operation of the SI is the normalized radial pressure gradient β , sometimes referred to as the headwind parameter, given by

$$\beta = -\frac{1}{2} \left(\frac{c}{v_K} \right)^2 \frac{\partial \ln p}{\partial \ln r}, \quad (2)$$

where v_K is the local orbital velocity and the pressure $p = \rho c^2$. This definition follows from the definition of the η parameter found in Eq. (8) of Cuzzi et al. (1993). However, for this work we use the background pressure gradient Π defined by the normalized difference between the local orbital velocity and the pressure supported

azimuthal gas velocity, βv_K as (e.g., Carrera & Simon 2022)

$$\Pi = \frac{\beta v_K}{c}. \quad (3)$$

We define Z_c to be the critical metallicity (or critical solids abundance, e.g. see Lesur et al. 2022) above which the SI is predicted to lead to sufficiently large amplitude gravitationally bound overdensities. While these critical metallicities are under some debate (U+20; Carrera & Simon 2022), Z_c is generally found to be a function of St , Π and α . The occurrence or absence of strong SI depends on whether or not the particle-gas layer experiences external turbulent forcing or self-generated dusty-gas instabilities.

Based on analysis of SI simulations without any external turbulent forcing (*i.e.* globally laminar yet turbulent due to dusty-gas midplane layer instabilities), Sekiya & Onishi (2018) conjecture that the relevant parameter determining strong activity is Z/Π , and its critical marginal value Z_c is only a function of St . In this respect there are three proposed occurrence diagrams based on a series of globally laminar axisymmetric and fully 3D simulations. The first two of these are based on the simulations of C+15 in which

$$\log \left(\frac{Z_c}{\Pi} \right) = 0.2 (\log \text{St})^2 + 0.59 \log \text{St} - 0.27, \quad (4)$$

and Y+17, with

$$\log \left(\frac{Z_c}{\Pi} \right) = 0.1 (\log \text{St})^2 + 0.2 \log \text{St} - 0.46, \quad (5)$$

(see also Carrera & Simon 2022). The third of these is based on LY21 who report that the range of SI activity in their globally laminar models is greatly expanded to include substantially lower values of Z for $\text{St} > 0.015$. They propose that

$$\log \left(\frac{Z_c}{\Pi} \right) = \begin{cases} 0.1 (\log \text{St})^2 + 0.32 \log \text{St} - 0.24; & \text{St} < 0.015; \\ 0.13 (\log \text{St})^2 + 0.1 \log \text{St} - 1.07; & \text{St} > 0.015 \end{cases} \quad (6)$$

The corresponding occurrence or absence of strong SI in the presence of external sources of turbulence is, like the laminar-case critical metallicities above, also subject to debate with no current consensus on the matter (e.g, U+20; Chen & Lin 2020; Gole et al. 2020; Schäfer et al. 2020). The uncertainty centers on the character of the underlying turbulence, e.g., where and on what scales is it mainly isotropic or strongly anisotropic (see recent mention in SJ22). In addition to the occurrence in Eq.

(6), LY21 (see their section 3.3.2) have also suggested an analogous relationship for Z_c that explicitly takes into account the degree of turbulence present in terms of the α parameter. Symbolically distinguished here as $Z_{c,\alpha}$, this criterion is based on simulations reported both in their study of self-generated SI turbulence and that of Gole et al. (2020) who considered the formation of overdensities in a model of the SI submerged in an externally driven turbulent fluid. It was proposed that

$$\frac{Z_{c,\alpha}}{\Pi} = \epsilon_c(\text{St}) \sqrt{\frac{1}{25} + \frac{\alpha/\Pi^2}{\alpha + \text{St}}}, \quad (7)$$

in which it is assumed that the laminar critical solids-to-gas ratio ϵ_c also applies in the presence of external sources of turbulence:

$$\log \epsilon_c(\text{St}) = \begin{cases} \log(2.5); & \text{St} < 0.015; \\ 0.48 (\log \text{St})^2 + 0.87 \log \text{St} - 0.11; & \text{St} > 0.015 \end{cases} \quad (8)$$

In this treatment we see that, for a given St , the effect of including a source of external turbulence is to shift the region of SI activity upwards. However, we note a caveat that this extension of the laminar case neglects some of the physics of turbulence in pp-disks such as radial diffusion which, for instance, is included in the solutions of U+20, and which becomes increasingly important for decreasing St .

SJ22 also propose $Z - \text{St}$ threshold boundaries for strong acting SI inferred from global axisymmetric simulations of the VSI in the presence of particles. We focus on their so-called “*SIafterVSI*” suite of simulation runs in which the VSI is allowed to develop before particles of a selected St value are added into a given numerical experiment. We do this mainly for two reasons: (1) because such a modeled scenario is more realistic as the VSI is likely well developed and turbulent before sub-micron sized grains can grow to the targeted St (e.g., E+22, also Sec. 4.1); and, (2) of the various models examined in SJ22 those of the *SIafterVSI* batch envision a wider area of $Z - \text{St}$ parameter space predicting strong acting SI in the presence of VSI turbulence. Based on earlier published simulations of similar setup (Schäfer et al. 2020) the VSI-SI complex appears to lead to $\alpha = \mathcal{O}(10^{-4})$ for the $0.005 \leq Z \leq 0.02$ values examined¹. We will adopt this value forthwith when considering the VSI.

Equations (4-8) define the so called SI occurrence boundaries. SJ22 do not provide an occurrence fit

like the ones discussed previously, and only sketch the boundaries of this active zone to be simultaneously greater than $\text{St} = 0.01$ and $Z = 0.0025$ with a straight line connecting the parameter pairs $(\text{St}, Z) = (0.015, 0.01)$, $(0.1, 0.0025)$ on a semilog graph. The simulations reported in SJ22 are characterized by values of the background pressure gradient given by $\Pi = 0.082 (r/10 \text{ au})^{1/4}$. We have translated this proposed occurrence boundary and expressed it in terms of Z/Π and St as part of our analysis in Sec. 4.

3. GLOBAL MODELS

In this paper we analyze a subset of pp-disk simulations from the recent work of E+22 (see also Estrada & Cuzzi 2022). These models use our 1+1D global nebula evolution code (Estrada et al. 2016) which includes the self-consistent treatment of growth and radial drift of all sizes, accounts for the vertical settling and diffusion of smaller grains, radial diffusion and advection of multiple species in solid or vapor phase, and contains a self-consistent calculation of the opacities and temperature (which depends on the evolving size distribution) that allows one to track the evaporation and condensation of all refractories and volatiles as they are transported throughout the gas disk (see also Sengupta et al. 2022).

E+22 have used this model to do a comprehensive study comparing compact particle and porous aggregate growth and drift over a range of disk conditions for a $1 M_\odot$ star, by including a model for fractal aggregate growth and compaction due to collisional (Okuzumi et al. 2012; Suyama et al. 2012) and non-collisional effects (Kataoka et al. 2013; Krijt et al. 2015). We select simulations from this work with both compact and fractal aggregate growth for global turbulent intensities of $\alpha = 10^{-3}$ and $\alpha = 10^{-4}$. These comprise a reasonable range of α -values consistent with observational indications that suggest that turbulence in pp-disks may be at the level of $10^{-4} < \alpha < 10^{-3}$ (e.g., Teague et al. 2016; Flaherty et al. 2017, 2018). The new aspect here is that these simulations (specifically models sa3g, fa3g, sa4g, fa4g; see Table 2 of E+22) have been evolved further from 0.5 Ma to 1 Ma to provide a sufficiently long baseline for our purposes.

The initial conditions for these models are derived from the analytical expressions of Lynden-Bell & Pringle (1974) as generalized by Hartmann et al. (1998) in terms of disk mass and turnaround radius (initially ~ 10 au) where the mass flux changes sign. The initial disk mass for these models is $0.2 M_\odot$ with a total metallicity of $Z \simeq 0.014$. The initial gas surface density is fairly compact similar to that of Desch (2007), and the disks are warm, with the temperature dependent on viscous dis-

¹ We note here that the turbulent intensity of the VSI has been shown by Lin (2019, and see also Lehmann & Lin 2022) to weaken as the particle loading increases.

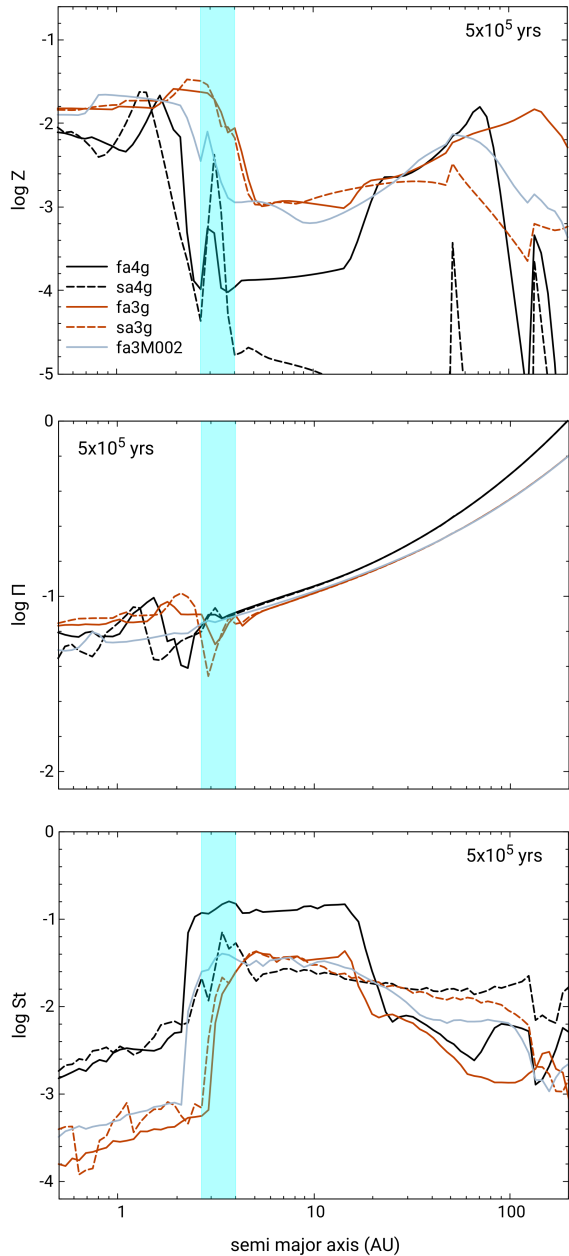


Figure 1. Local disk metallicities Z , normalized pressure gradient Π , and the mass dominant particle Stokes number St for all models as a function of semi-major axis after 0.5 Ma. Fractal growth models are given by solid curves, and compact particle growth models by the dashed curves. The shaded cyan region demarcates the radial range over which the water snowline is located after this time. Regions of enhancement in Z are generally outside evaporation fronts (see Estrada & Cuzzi 2022). One additional lower disk mass model (grey curves) of $0.02 M_{\odot}$ (fa3M002g), ten times lower than model fa3g, is included for comparison.

sipation and a time variable stellar luminosity which is roughly an order of magnitude higher than solar at the beginning of the simulations. This places the water snow

line initial location between $\sim 10 - 15$ au and is meant to represent early (Class I) pp-disk conditions immediately following the infall stage (see, e.g., Drażkowska & Dullemond 2018; Homma & Nakamoto 2018). Detailed discussion of the initial conditions can be found in E+22.

Figure 1 provides a snapshot of these simulations after 0.5 Ma of evolution. We plot the local metallicity Z (top panel), the normalized pressure gradient Π (middle panel) and the *mass dominant* particle and aggregate Stokes numbers (bottom panel) for both fractal aggregate (solid curves) and compact particle (dashed curves) growth models as a function of location in the disk. By mass-dominant, we mean the particle size (mass) defined by the mass weighted mean of the distribution. Our simulations have size distributions that range from a 0.1 micron monomers to the largest particle and aggregate size reached before growth frustration due to bouncing, fragmentation, and/or radial drift sets in. Though their St may be similar, the underdense fractal aggregates can be quite large compared to their compact counterparts (see Appendix of E+22).

As noted by E+22, a general difference between fractal and compact particle growth models is that radial drift is less of a factor for porous aggregates over a significant fraction of their growth phase due to a combination of initially pure fractal growth and then slow compaction, while the St of the compact particles increase more quickly and are subject to stronger radial drift earlier on. Eventually fractal aggregates can grow much faster due to their larger cross sections. This behavior generally explains the difference between compact and fractal models in Z , especially outside of ~ 20 au (Fig. 1, upper panel). The difference in St (lower panel) inside and outside the water snowline (the cyan region across these models between $\sim 2.8 - 4$ au after this time) is due to water ice being more sticky, which allows water ice-bearing aggregates to grow much larger before becoming fragmentation or drift limited.

It is important to understand the variation in the local metallicity Z . Enhancements in the local metallicity (found to reach values as high as $Z \sim 0.05$ in these models) arise primarily due to the radial drift of particles and aggregates across evaporation fronts (EFs). Inward drifting particles can lose most or all of their associated volatile enhancing the vapor phase inside the EF. This vapor can subsequently diffuse (or advect) outwards back across the EF and recondense, enhancing the solids abundance there. In cases of low α and/or at longer times, these enhanced regions can appear as “bands” dominated by the associated volatile, most notably for the compact growth model sa4g for $\alpha = 10^{-4}$ in the top panel of Fig. 1 (see also Fig. 6, upper right

panel of Estrada & Cuzzi 2022, and for more detailed discussion).

4. INTERPRETATION OF RESULTS IN TERMS OF SI

4.1. Temporal Trajectories of Particle Growth and Disk Evolution

In Figure 2, we plot the temporal trajectories of particle St and Z/Π over 1 Ma for the models introduced in Sec. 3. Each of the trajectories for the indicated radial locations in the disk (1, 3, 5, 10 and 30 au) begin far off to the left on the x -axis. A typical monomer in the regions of interest have $St \sim 10^{-9}$, though this will depend on the gas surface density. Growth rates vary throughout the disk, but at 1 au for instance where growth rates are more rapid, St can increase by a few orders of magnitude in only 100 orbits² for the compact growth model, while the initially slower growing fractal aggregates have St an order of magnitude smaller than the compact case after the same time.

The sharp increases (or decreases) in Z/Π seen along the trajectories can be associated with multiple refractory species' EFs inside the snowline (e.g., silicates, FeS, see Estrada & Cuzzi 2022) which should be understood to be evolving inwards as the disk cools with time. Recondensing volatiles from the migrating particles that cross these EFs can lead to enhancements in solids outside them (Sec. 3), stimulating growth to larger St there. For example, the large variation in Z/Π seen at 3 au in the compact growth case for $\alpha = 10^{-4}$ is due to the water snowline evolving through this radius. As discussed in Sec. 3, this particular model (see Fig. 1, upper panel) is characterized by bands of enhancements which can be orders of magnitude higher than the background Z . As the EF migrates inwards, the location of these bands also move inwards explaining the even more sharp decrease in Z/Π relative to the other models.

Interestingly, simulations with the higher $\alpha = 10^{-3}$ tend to have larger Z/Π than the lower α case and which persist for longer periods of time. The inward migration of the EFs from the water snowline and inward is slower for $\alpha = 10^{-3}$ because for this level of turbulence the inner disk stays hotter longer due to combination of particle size and opacity (e.g., see Fig. 1, Estrada & Cuzzi 2022). As a result this can lead to larger local metallicity. For $\alpha = 10^{-4}$, cooling is more rapid because the mass dominant aggregates grow quickly to

higher St leading to lower opacities, and faster drift, so enhancements do not get quite as large.

Overall, the general trend across these models is that as particles and aggregates grow and their St increases, radial drift becomes faster leading to a sharp, concurrent decrease in the metallicity near large St regions so that having both large St and Z for $\alpha \geq 10^{-4}$ is prevented. Thus for this epoch, $\epsilon < 1$, always. This behavior in our simulations differs from other published work that in some cases find that conditions for the SI can be satisfied (*i.e.*, $\epsilon = \mathcal{O}(1)$) for these turbulent intensities. We summarize some key differences between our models and others in the Appendix.

4.2. Turbulence and SI

Also plotted in Fig. 2 are the SI occurrence boundaries previously advocated by others for the critical Z_c (dashed curves) defined by Eqs. (4-6), and for $Z_{c,\alpha}$ (solid curves) defined by Eqns. (7-8). Our particle growth simulations tended to achieve Π values lying within a well-defined range $0.05 < \Pi(r, t) < 0.22$ (corresponding to the inner disk region, and ~ 100 au, respectively). As such, we always depict two $Z_{c,\alpha}$ curves corresponding to these two extreme values of Π . All curves for $Z_{c,\alpha}$ and Z_c are specifically labeled in the legend in the top left panel. We see that although there are instances where curves for Z_c are crossed (e.g., top right panel), those crossed apply only to laminar disks (in which the only turbulence is self-generated by the particle layer). We find quite generally that there are no cases where the temporal trajectories of particle growth in turbulence, in either fractal or compact cases, cross the critical curves $Z_{c,\alpha}$ which have been proposed for globally turbulent pp-disks like those we examine here.

The boundaries in parameter space defining the occurrence or absence of strong acting SI under turbulent conditions remain unsettled. The three studies (C+15; Y+17; LY21) described in Sec. 2 established the occurrence boundaries in Z, Π and St by analyzing direct numerical simulations of the SI in globally non-turbulent nebulae and querying whether a given numerical experiment generates particle overdensities that exceed the Roche-density condition for gravitational binding. If these requisite conditions are met, then the SI is considered to be strong enough to lead to planetesimals. But these criteria only apply when there is no external source of turbulence.

We do note that even these proposed criteria appear to be violated in some instances like in the recent study of Carrera & Simon (2022), who considered the SI in a model with low St ($= 0.015$, 1 mm-sized compact grains) in a globally non-turbulent disk, but experi-

² Note that well developed VSI is found to occur in < 100 orbital periods (Richard et al. 2016).

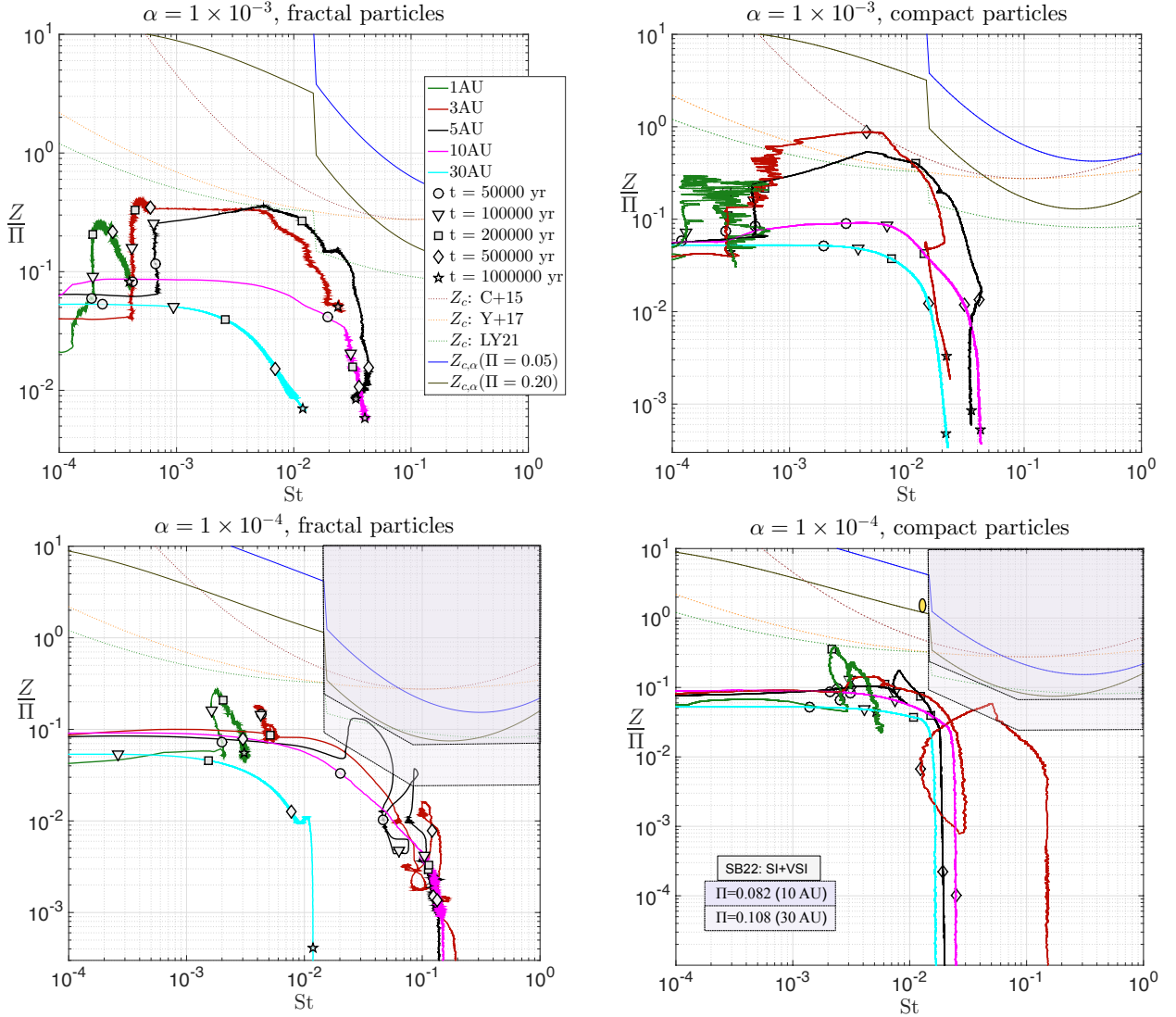


Figure 2. Temporal trajectories in $Z/\Pi - St$ parameter space for the global pp-disk evolution models with compact particle and fractal aggregate growth discussed in Section 3. Trajectories for each model (which begin far off to the left) are plotted at 1, 3, 5, 10, and 30 au spanning 1 Ma for each simulation: (upper left) fractal particles and $\alpha = 10^{-3}$; (upper right) compact particles and $\alpha = 10^{-3}$; (bottom left) fractal particles and $\alpha = 10^{-4}$; (bottom right) compact particles and $\alpha = 10^{-4}$. These correspond to models fa3g, sa3g, fa4g, and sa4g, respectively, in Fig. 1. Also shown are the predicted critical curves Z/Π as a function of St , Π and α based on Eqns. (7-8). In the bottom panels, we additionally show the occurrence region predicted from the simulations of SJ22 for two values of Π as indicated in the bottom right legend. Open symbols along the trajectories mark the associated times in the upper left legend.

encing settled particle layer generated turbulence with $\alpha \approx 6 \times 10^{-5}$. They found that no sufficiently large gravitational overdensities were produced in the (settled layer driven) turbulently active part of the simulation, where locally $Z/\Pi \approx 1.06$ and $0.028 < \Pi < 0.030$. The lower row (right panel) of Fig. 2 designates the position in parameter space of this simulation with a vertically elongated orange oval that lies well above the appropriate criteria Z_c based on purely self-generated turbulence, Eqns. (4-6, dashed lines), suggesting that

strong overdensities should occur. Yet, according to the corresponding externally-driven turbulence occurrence prediction of LY21, Eqns. (7-8, solid lines), this simulation is not expected to produce gravitationally bound overdensities. Carrera & Simon (2022) offer a different interpretation for this outcome. According to their *residence time* idea, the SI might well be on its way toward producing gravitationally bound overdensities in the particle field but that there is not enough time for

it to fully develop before the particles radially drift into that part of the disk where the SI ceases to operate.

One should also consider a corresponding weak criterion based on SI growth rate estimates in the face of turbulence like the α -disk turbulence models of U+20 and Chen & Lin (2020), where it is envisioned that SI derived high density filaments actually grow out of a largely isotropic turbulent state driven by some process other than the SI itself – a proposition supported by recent re-examination of particle-laden turbulence in pp-disk midplanes (see Sengupta & Umurhan 2023). We propose this to be a weak bookend criterion simply on the fact that not all SI unstable settings are expected to lead to gravitationally bound overdensities. As the thinking goes, if the isotropic turbulence is so strong that predicted SI growth rates are thousands of orbit times or longer, then it would be justifiable to conjecture that the SI is either very weak or practically inactive. U+20 in fact show for the parameter combination $St \lesssim 0.1$ and α large enough that the midplane values of $\epsilon \equiv \rho_{\text{solids}}/\rho \leq 1$ (*i.e.*, the so-called Zone II region of the $\alpha - St$ parameter plane) that the predicted growth rates are not only very long, but also (of the few simulations reported in the literature that were conducted in that parameter range) indeed show no appreciable action driven by the SI for the plausible and simple reason that growth timescales exceed drift loss times.

The framework laid out in U+20, suggests that the SI should be strong when the growth times are short compared to loss times – that is to say, acting on $\mathcal{O}(1)$ orbital timescales – consistent with the simulations that lead to the emergence of strong high density filaments as reported by C+15 and Y+17. As shown in U+20, as well as in E+22, none of the detailed particle evolution (growth + drift) models run for values of $10^{-4} \leq \alpha \leq 10^{-3}$ ever generate parameter combinations that predict turbulent SI growth rates less than several hundreds to thousands of orbit timescales. This general weakness in predicted turbulent SI growth rates is due to the fact that the simulations never produce mass-bearing particles with St values much exceeding $\sim 0.03 - 0.04$. For the models presented here we *do* find instances where $St \sim 0.1$; however, as St increases, the local values of Z concurrently decrease to extremely low values ($\ll 0.01$). The turbulent SI growth rates under these conditions are also extremely long according to the theoretical framework of U+20 and Chen & Lin (2020) except for when St begins to approach and/or exceed 0.1.

Moreover, the particles themselves are also likely coming up against the radial drift barrier (and indeed, this is why local Z decreases more quickly) in which predicted

growth timescales are the same order of magnitude or longer than the radial drift timescales across the disk – an argument in the same spirit as Carrera & Simon (2022)’s residence time interpretation.

To examine this competition, we show in Figure 3 the U+20 predicted growth timescales, t_g , for the case where $Z = 0.001$. This metallicity value is chosen since it corresponds to an upper Z bound of our simulations during late times – roughly after 0.2 Ma – and that which corresponds to largest St values achieved, *i.e.*, around $\mathcal{O}(0.1)$ for models fa4g and sa4g. Overlain on Figure 3 are the timescale limits for radial drift, t_d , based on Eq. (25) of U+20, and reproduced here in terms of orbital time units $P_{\text{orb}} \equiv 2\pi/\Omega$:

$$t_d = \frac{(1 + \epsilon)^2 + St^2}{4\pi St \cdot \Pi^2} P_{\text{orb}}, \quad \epsilon \approx Z \sqrt{\frac{\alpha + St}{\alpha}}, \quad (9)$$

in which the relationship for ϵ is a robust estimate based on the balance of downward vertical particle settling and upward turbulent particle diffusion (e.g. Dubrulle et al. 1995). Figure 3 also designates the range of α and St values broadly characterizing the particle growth simulations reported here. We find that for values of $St \lesssim 0.01$ neither the low or high α values should lead to linearly unstable turbulent SI growing on timescales shorter than t_d . However in the range $0.01 \lesssim St \leq 0.1$ there appears a region in the $\alpha - St$ parameter plane, which is bounded below by the line $\alpha = 10^{-4}$ and above by the relationship $\alpha \approx 0.01 St$, in which $t_g < t_d$. In this patch of allowable parameter space we find that $t_g \geq 350 P_{\text{orb}}$, wherein equality occurs for $\alpha = 10^{-4}$ and $St \approx 0.1$. We suggest therefore that under these Z -rarefied conditions (which occur for a brief period in the models for $\alpha = 10^{-4}$ when $Z/\Pi \gtrsim 10^{-2}$, see 3 au trajectories in Fig. 2) that the SI might possibly lead to relatively high density particle filaments inside this parameter region, but we suspect that because of the relatively slow growth rates it is not expected to lead to gravitationally bound overdensities.

Lastly, we have included the proposed occurrence boundary predicted by SJ22 from their *SIafterVSI* simulations translated to $Z/\Pi - St$ space for two values of their assumed Π at 10 and 30 au. The occurrence zone is shown as two shaded regions found on the bottom panels of Fig. 2 for the cases with $\alpha = 10^{-4}$ which is the most appropriate comparison. The first value corresponds to the inner boundary of their simulations, while the second is used as a direct comparison with our 30 au trajectory. It can be seen that although these represent a marked improvement for the favorability of the SI in the presence of a source of external turbulence, the boundaries still lie well above their respective temporal trajectories for 10 (magenta curves) and 30 au (cyan

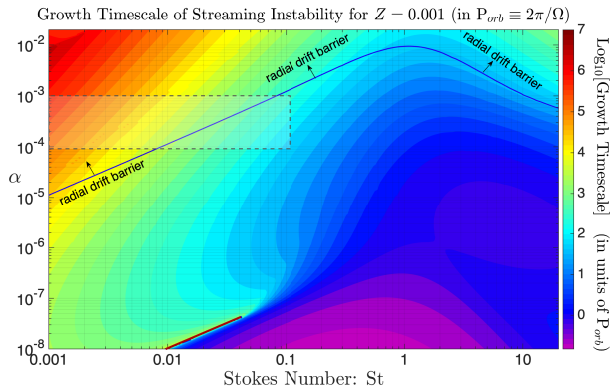


Figure 3. SI growth timescales (t_g) as a function of α and St , with $Z = 0.001$ and $\Pi = 0.05$, based on U+20 under the assumption of isotropic turbulence. The hatched box region in upper left demarcates the parameter region generally encompassing those achieved in the simulations reported here. The figure shows a curve corresponding to the region of parameter space in which $t_d = t_g$ and designates with arrows where $t_d < t_g$, where t_d is the drift time. There exists a putative range within the hatched region in which $t_d > t_g$, but even here growth times are long (see text for further details).

curves) which are already steeply decreasing in Z for $St \gtrsim 0.01$.

3D numerical simulations of the VSI conducted on large radial domains predict that its unsteady/turbulent dynamics are strongly anisotropic (e.g. Stoll et al. 2017; Flock et al. 2017, 2020), with unsteady vertical motions dominating corresponding radial motions. SJ22 observe that the anisotropic character of VSI turbulence, and its inherently weak attendant radial momentum and particle diffusions, helps to rationalize why the SI can lead to gravitationally bound overdensities in VSI turbulent disks even with moderate turbulence levels ($\alpha \sim 10^{-4}$) and relatively small effective St (in the range of 0.006 and 0.06). By contrast, the SI subject to isotropic turbulence – yet under otherwise similar St and α measures – is predicted to be weakened by comparison (Chen & Lin 2020; Umurhan et al. 2020; Gole et al. 2020). We understand this to be because the radial diffusion of particles and momentum are of similar order magnitude as that in the vertical direction, which implies that radial diffusion should act against the ready formation of filaments³.

Indeed, a preliminary spectral kinetic energy analysis of the VSI in the radially relatively large domain, fully 3D, numerical experiment reported in Flock et al.

³ U+20 show that the fastest growing modes generally correspond to relatively short radial wavelength disturbances compared to the vertical, especially under moderate values of turbulent intensity and values of $St < 0.1$.

(2020) shows tell-tale signs of Kraichnan-Batchelor dual cascade in the gaseous kinetic energy, whose characteristic inverse energy cascade likely goes in part toward explaining the observed strong anisotropy in well-developed VSI simulations – especially with respect to its predominant vertical motions – as well as the emergence of prominent large-scale z -direction oriented vortices in sufficiently global disk models. (similarly in VSI simulations of Manger et al. 2021)

It is worth commenting that Flock et al. (2020) show the kinetic energy distribution (\mathcal{E}_m) on the spectrum of azimuthal wavenumbers (m) within a restricted annular regime of their full simulation. They find a $\mathcal{E}_m \sim m^{-3}$ dependence on lengthscales shortward of a characteristic scale $\lambda_0 \equiv 2\pi R/m_0$, and a $\mathcal{E}_m \sim m^{-5/3}$ shape longward of λ_0 . This feature is emblematic of Kraichnan-Batchelor double cascade character of 2D turbulence driven at a length scale λ_0 (Boffetta & Ecke 2012; Alexakis & Biferale 2018), where energy propagates toward scales larger than λ_0 , while enstrophy propagates toward scales smaller than λ_0 . Close inspection of the simulation discussed would show that the lengthscale λ_0 corresponds to the emergence of radially/azimuthally shortened but vertically elongated columnar vortices (e.g., see Fig. 5 in Flock et al. 2020). In accordance with an inverse-energy cascade dynamic, we think that given enough time these vortices merge with one another to ultimately bring about the aforementioned azimuthally extended large-scale steady vortices seemingly characteristic of well-developed VSI.

Whether the VSI is truly quasi-2D in dynamical character or, perhaps, dynamically more akin to flows exhibiting a split-cascade remains to be determined only once higher resolution simulations are conducted that capture its fastest growing linear modes with lengthscale λ_{\max} . For the VSI $\lambda_{\max} = \mathcal{O}(H^2/R)$ (Urpin 2003; Umurhan et al. 2016; Yellin-Bergovoy et al. 2021), which needs at least 20-40 grid point resolution across λ_{\max} to numerically resolve any potential downscale energy cascade (for instance, see the relative high resolution but radially restricted VSI simulations of Richard et al. 2016).

On the other hand, if the disk is subject to ZVI turbulence (Zombie Vortex Instability, Marcus et al. 2013; Barranco et al. 2018), then its turbulence is known to be more isotropic (e.g. Marcus et al. 2016) expressing a classical Kolmogorov $k^{-5/3}$ spectrum down to the smallest dynamically resolvable and non-artificially dissipating scales. Under such driving, using an isotropic turbulence model – like the simple mixing-length α -disk form often used – would be more appropriate to predict how the SI develops under turbulent forcing. Thus,

assessing how the SI fares under realistic and properly resolved numerical models of disk turbulence, whether it be driven by the VSI or something else, remains an open issue needing elucidation in the near term.

5. SUMMARY

We analyze previously conducted self-consistent particle growth simulations of E+22 for both fractal and compact aggregates in the presence of global turbulence with values of $\alpha = 10^{-4} - 10^{-3}$ in order to evaluate whether conditions for the SI to produce gravitationally bound particle overdensities can be achieved in the earliest stages ($\lesssim 1$ Ma) of globally evolving pp-disks, an epoch in which meteoritic and observational evidence strongly suggest that planetesimals have already formed. For this work, the selected simulations have been extended from 0.5 Ma to 1 Ma in order to provide a long enough baseline such that the likelihood for strong and efficient acting SI to arise is systematically moving in the direction of lower probability after these times.

As input, we utilize the time series generated during each simulation that track the change in the relevant properties, namely the local metallicity Z , the mass-dominant particle or aggregate St , and the pressure gradient as a function of semi-major axis in the disk. We then compare temporal trajectories for several radial locations of interest of the constructed Z/Π from these with the SI occurrence boundaries in Z , Π and St (Eqns. 4-8) from four recent studies (C+15; Y+17; LY21; SJ22) established via analysis of numerical simulations of the SI. The bulk of these occurrence boundaries only apply to globally laminar disks; however, LY21 also proposed an extension of this formalism, $Z_{c,\alpha}$, envisioned to apply to a globally turbulent pp-disk, while SJ22 also predicted an occurrence boundary based on their simulations of the VSI, both of which we have used here to compare with our models of turbulent particle growth.

We find quite generally within the first Ma of evolution that there are no times for any of the analyzed models where the temporal trajectories at the selected radial locations in $Z/\Pi - St$ space comes near exceeding $Z_{c,\alpha}(\Pi, St, \alpha)$, which defines the critical solids abundance for planetesimal formation by the SI proposed by LY21 in the presence of external turbulence. Furthermore, the temporal trajectories for the compact and fractal growth models with $\alpha = 10^{-4}$ also do not come near the boundaries predicted by SJ22 in the presence of the VSI despite conditions being more favorable for the SI compared to LY21. The main reason for this is that as growth proceeds to larger St values, particles are subject to rapid radial drift, and the local metallicity con-

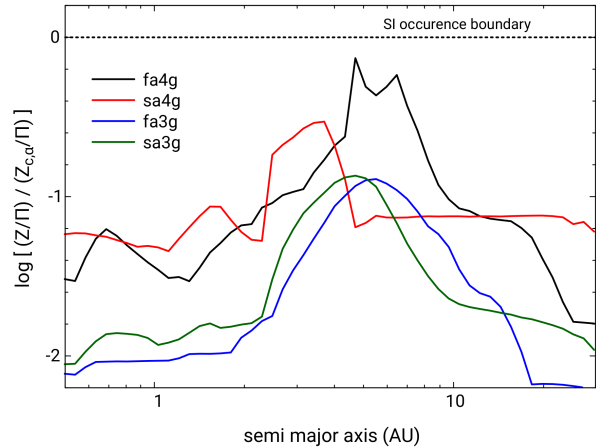


Figure 4. Maximum value for the ratio of Z/Π and $Z_{c,\alpha}/\Pi$ from 0.5 to 30 au over 1 Ma for all models considered. To generate these curves, the models’ evolving $St(t)$ and $\Pi(t)$ at each radial location are input into Eq. 7 and compared with the models’ Z/Π over all times t to find the maximum. Each radial location reaches its maximum value at different times and has a different St associated with it. Crossing the SI occurrence boundary (black dotted curve) requires a ratio larger than unity. The largest value occurs in the fractal aggregate model (fa4g) for $\alpha = 10^{-4}$ near 5 au (*cf.* Fig. 2) between 30 and 40 kyr. The trend outside of 30 au continues to be the same because Z/Π decreases, and St remain small (though photoevaporation may change these trends at later times, e.g., Carrera et al. 2017)

currently decreases sharply to small values ($Z \ll 0.01$), veering trajectories away from the SI occurrence regions.

This result, which applies to both the compact particle and fractal aggregate growth models, is consistent with the predictions of U+20, and E+22 where the straightforward $\epsilon \gtrsim 1$ constraint is applied. Though we have selected specific radial locations in Fig. 2 to demonstrate the temporal trajectories of particle growth and local metallicity explicitly, other radial locations produce similar results, as is summarized in Figure 4 where for each radial location we plot the maximum value of each model’s Z/Π -to- $Z_{c,\alpha}/\Pi$ ratio (Eq. 7) achieved over the full 1 Ma course of a simulation. In this format it is easier to visualize that in order to breach the SI occurrence region, this ratio must exceed unity which does not occur for any of our models analyzed here (see figure caption).

There are instances where the particle $St \gtrsim 0.1$, which are associated with a small local Z owing to fast radial drift. U+20 only briefly discussed the growth rates for the SI in the context of their theory for a low value of $Z = 0.001$, and here we find that for this Z the growth rates (Fig. 3) are indeed long except when one approaches $St \sim 0.1$ for $\alpha = 10^{-4}$, in which the e-folding timescales are on the order of several hundred orbits and

shorter than the radial drift timescales of the particles. It is thus feasible that the SI could be active in this epoch under these conditions, though presumably only weakly so, based on the long growth times. Whether such conditions could generate planetesimals for these parameters over such long growth times requires addressing with appropriately constructed future numerical simulations.

Finally, we should acknowledge that our results here for the models we have considered do not preclude the operation of the SI at later times when the disk has evolved significantly more due to, for example, open-system loss processes such as winds (see, e.g., Sengupta et al. 2022). For instance, removal of the disk gas via photoevaporation (e.g., Carrera et al. 2017) would lead to an environment where increasing particle St as a result of decreasing gas density may achieve the $Z - St$ conditions for planetesimal formation via SI, perhaps explaining the formation of KBOs (Nesvorný et al. 2019), but these would form much later than the epoch addressed in this work. Along the same lines, low gas mass, very cold disk conditions are more conducive to strong SI, but like the photoevaporative case above these conditions may most often be associated with older, Class II, evolved disks which is not our focus.

Acknowledgements. The authors acknowledge fruitful discussions with the TCAN collaboration including W. Lyra, J. Simon, C.-C. Yang, and A. Youdin, as well as D. Carrera and S. Bonnet. We also thank J. Cuzzi and D. Sengupta for their valuable input, and to an anonymous reviewer whose suggestions helped to improve this paper. We are grateful for the “Planets in the Desert” workshop during June 2022 at New Mexico State University that set the scene for us to conduct this study.

APPENDIX COMPARISON TO PUBLISHED RESULTS

A reviewer asked that we stipulate the main ways in which our models differ from others in the literature beyond just model parameter choices. We do not attempt an exhaustive comparison here and, instead, consider several studies published over the last decade. In many cases differences can be distilled down to others’ use of simplified, monodisperse growth models in a globally turbulent disk where the *largest* particle growth time is taken to be $\tau_{\text{grow}} = a/\dot{a} \simeq 1/(Z\Omega)$, and in which the SI is *assumed* to operate whenever $St \geq 0.01$ and $\epsilon = \mathcal{O}(1)$ (e.g., Drażkowska et al. 2016; Drażkowska & Alibert 2017; Carrera et al. 2017; Schoonenberg et al. 2018; Charnoz et al. 2019; Morbidelli et al. 2022). Once

these SI criterion are met, it is then assumed that planetesimals form at a somewhat arbitrary rate.

The parameterization for τ_{grow} cited above leads to overall much faster growth than in our models mainly because it assumes perfect sticking up to the fragmentation barrier (and/or drift barrier). Moreover, in deriving the approximation τ_{grow} it is also assumed that particles are always in the Epstein regime (all simulations analyzed here have a fraction, and in some cases sizeable, of particles in the Stokes regime, see E+22), and that $St \gg \alpha$ even in the initial growth stages. These approximations mean τ_{grow} itself is always independent of particle size (or St). Though a useful tool, these simplified growth models cannot fully capture the complexities that can arise using more detailed coagulation models, and indeed it is known that they deviate from them (e.g., see Lenz et al. 2020).

Other models largely ignore particle bouncing as well, even though Zsom et al. (2010, also, Güttler et al. 2010) showed that it is a significant barrier to growth. In our model, we do not assume instantaneous fragmentation at some threshold relative velocity, but rather treat fragmentation and bouncing together using a mass- and velocity-dependent sticking coefficient (e.g., see also Okuzumi & Hirose 2012; Homma et al. 2019; Estrada et al. 2016), which can increasingly slow the growth rate as the fragmentation barrier is approached because the largest particle can only grow efficiently from a relatively diminishing feedstock. This approach is much more restrictive, but we believe it to be more realistic than assuming perfect sticking up to the fragmentation (or drift) barrier. Naturally, slower growth makes overcoming the radial drift barrier even more challenging.

We also do not adopt the above-cited criteria for the onset of strong acting SI. While we consider the $\epsilon \gtrsim 1$ criterion to be necessary for strong SI, we generally rely on the more complete solutions and analytical theory of U+20, which successfully back-predicts a multitude of SI simulations in the literature as to whether they lead to SI rapidly growing out of a turbulent state. None of our global model cases analyzed in this paper are predicted to become strongly SI active from the analysis of U+20, and (in the sense of leading directly to planetesimals) we never reach those conditions. On the other hand, E+22 do find a global model case that develops $St \gtrsim 0.3$ and $\epsilon > 1$ – at the snowline and for *small* $\alpha = 10^{-5}$ – that also happens *to be* consistent with the predictions for strong acting SI according to U+20 theory.

Some other models simulate low gas mass, cold pp-disks (e.g., Gonzalez et al. 2017; Schoonenberg et al. 2018), which may be more appropriate for older and significantly evolved Class II objects. Such gas-rarefied en-

vironments are generally conducive for strong SI⁴. Note that the models of [Carrera et al. \(2017\)](#) begin massive, but they allow photoevaporation to remove disk gas. They find conditions for the SI are met in the outermost and innermost regions of their disk, but only at much later times when gas surface densities have decreased significantly (the local Z and St increase accordingly) effectively evolving to a Class II pp-disk.

Our model simulations are perhaps most similar to those of [Lenz et al. \(2020\)](#), and also [Homma & Nakamoto 2018](#); [Homma et al. 2019](#)) who use the full coagulation code of [Birnstiel et al. \(2010\)](#), also, [Brauer et al. 2008](#)); however, the main difference is that [Lenz et al.](#) assume

that “pebble traps” appear and disappear on some arbitrary timescale within which entrapped pebble clouds can collapse into planetesimals with some specified efficiency⁵. [Homma & Nakamoto \(2018\)](#) modeled the infall stage of the disk with fractal aggregate growth, and found that they could not form planetesimals outside the snow line, whereas [Homma et al. \(2019\)](#) assumed a sticky organics (“adhesion”) model with a larger fragmentation threshold in the inner disk to produce planetesimals. The peak masses of compact particles and porous aggregates achieved though in these models are similar to those we obtain in our simulations (see also, e.g., [Krijt et al. 2015](#)).

REFERENCES

- Alexakis, A., & Biferale, L. 2018, *PhR*, 767, 1, doi: [10.1016/j.physrep.2018.08.001](https://doi.org/10.1016/j.physrep.2018.08.001)
- Barranco, J. A., Pei, S., & Marcus, P. S. 2018, *ApJ*, 869, 127, doi: [10.3847/1538-4357/aaec80](https://doi.org/10.3847/1538-4357/aaec80)
- Birnstiel, T., Dullemond, C. P., & Brauer, F. 2010, *A&A*, 513, A79, doi: [10.1051/0004-6361/200913731](https://doi.org/10.1051/0004-6361/200913731)
- Boffetta, G., & Ecke, R. E. 2012, *Annual Review of Fluid Mechanics*, 44, 427, doi: [10.1146/annurev-fluid-120710-101240](https://doi.org/10.1146/annurev-fluid-120710-101240)
- Brauer, F., Dullemond, C. P., & Henning, T. 2008, *A&A*, 480, 859, doi: [10.1051/0004-6361:20077759](https://doi.org/10.1051/0004-6361:20077759)
- Carrera, D., Gorti, U., Johansen, A., & Davies, M. B. 2017, *ApJ*, 839, 16, doi: [10.3847/1538-4357/aa6932](https://doi.org/10.3847/1538-4357/aa6932)
- Carrera, D., Johansen, A., & Davies, M. B. 2015, *A&A*, 579, A43, doi: [10.1051/0004-6361/201425120](https://doi.org/10.1051/0004-6361/201425120)
- Carrera, D., & Simon, J. B. 2022, *ApJL*, 933, L10, doi: [10.3847/2041-8213/ac6b3e](https://doi.org/10.3847/2041-8213/ac6b3e)
- Chambers, J. E. 2014, *Icarus*, 233, 83, doi: [10.1016/j.icarus.2014.01.036](https://doi.org/10.1016/j.icarus.2014.01.036)
- Charnoz, S., Pignatale, F. C., Hyodo, R., et al. 2019, *A&A*, 627, A50, doi: [10.1051/0004-6361/201833216](https://doi.org/10.1051/0004-6361/201833216)
- Chen, K., & Lin, M.-K. 2020, *ApJ*, 891, 132, doi: [10.3847/1538-4357/ab76ca](https://doi.org/10.3847/1538-4357/ab76ca)
- Connelly, J. N., Bizzarro, M., Krot, A. N., et al. 2012, *Science*, 338, 651, doi: [10.1126/science.1226919](https://doi.org/10.1126/science.1226919)
- Cuzzi, J. N., Dobrovolskis, A. R., & Champney, J. M. 1993, *Icarus*, 106, 102, doi: [10.1006/icar.1993.1161](https://doi.org/10.1006/icar.1993.1161)
- D’Angelo, G., Henning, T., & Kley, W. 2003, *ApJ*, 599, 548, doi: [10.1086/379224](https://doi.org/10.1086/379224)
- Desch, S. J. 2007, *ApJ*, 671, 878, doi: [10.1086/522825](https://doi.org/10.1086/522825)
- Desch, S. J., Kalyaan, A., & O’D. Alexander, C. M. 2018, *ApJS*, 238, 11, doi: [10.3847/1538-4365/aad95f](https://doi.org/10.3847/1538-4365/aad95f)
- Drażkowska, J., & Alibert, Y. 2017, *A&A*, 608, A92, doi: [10.1051/0004-6361/201731491](https://doi.org/10.1051/0004-6361/201731491)
- Drażkowska, J., Alibert, Y., & Moore, B. 2016, *A&A*, 594, A105, doi: [10.1051/0004-6361/201628983](https://doi.org/10.1051/0004-6361/201628983)
- Drażkowska, J., & Dullemond, C. P. 2018, *A&A*, 614, A62, doi: [10.1051/0004-6361/201732221](https://doi.org/10.1051/0004-6361/201732221)
- Drażkowska, J., Li, S., Birnstiel, T., Stammer, S. M., & Li, H. 2019, *ApJ*, 885, 91, doi: [10.3847/1538-4357/ab46b7](https://doi.org/10.3847/1538-4357/ab46b7)
- Dubrulle, B., Morfill, G., & Sterzik, M. 1995, *Icarus*, 114, 237, doi: [10.1006/icar.1995.1058](https://doi.org/10.1006/icar.1995.1058)
- Dullemond, C. P., Birnstiel, T., Huang, J., et al. 2018, *ApJL*, 869, L46, doi: [10.3847/2041-8213/aaf742](https://doi.org/10.3847/2041-8213/aaf742)
- Estrada, P. R., & Cuzzi, J. N. 2022, *ApJ*, 936, 40, doi: [10.3847/1538-4357/ac81c6](https://doi.org/10.3847/1538-4357/ac81c6)
- Estrada, P. R., Cuzzi, J. N., & Morgan, D. A. 2016, *ApJ*, 818, 200, doi: [10.3847/0004-637X/818/2/200](https://doi.org/10.3847/0004-637X/818/2/200)
- Estrada, P. R., Cuzzi, J. N., & Umurhan, O. M. 2022, *ApJ*, 936, 42, doi: [10.3847/1538-4357/ac7ffd](https://doi.org/10.3847/1538-4357/ac7ffd)
- Flaherty, K. M., Hughes, A. M., Teague, R., et al. 2018, *ApJ*, 856, 117, doi: [10.3847/1538-4357/aab615](https://doi.org/10.3847/1538-4357/aab615)
- Flaherty, K. M., Hughes, A. M., Rose, S. C., et al. 2017, *ApJ*, 843, 150, doi: [10.3847/1538-4357/aa79f9](https://doi.org/10.3847/1538-4357/aa79f9)
- Flock, M., Nelson, R. P., Turner, N. J., et al. 2017, *ApJ*, 850, 131, doi: [10.3847/1538-4357/aa943f](https://doi.org/10.3847/1538-4357/aa943f)
- Flock, M., Turner, N. J., Nelson, R. P., et al. 2020, *ApJ*, 897, 155, doi: [10.3847/1538-4357/ab9641](https://doi.org/10.3847/1538-4357/ab9641)
- Garcia, A. J. L., & Gonzalez, J.-F. 2020, *MNRAS*, 493, 1788, doi: [10.1093/mnras/staa382](https://doi.org/10.1093/mnras/staa382)

⁴ It should be noted that in [Gonzalez et al. \(2017\)](#), see also [Garcia & Gonzalez 2020](#)), the mechanism proposed to lead to planetesimal formation is self-induced dust traps, and is different from the SI. The dust traps arise due to the combination of growth and fragmentation of dust grains coupled with the back reaction with the gas when $\epsilon = \mathcal{O}(1)$.

⁵ This mechanism for planetesimal formation is different from the SI, and might be more akin to turbulent concentration ([Hartlep & Cuzzi 2020](#)).

- Gole, D. A., Simon, J. B., Li, R., Youdin, A. N., & Armitage, P. J. 2020, *ApJ*, 904, 132, doi: [10.3847/1538-4357/abc334](https://doi.org/10.3847/1538-4357/abc334)
- Gonzalez, J. F., Laibe, G., & Maddison, S. T. 2017, *MNRAS*, 467, 1984, doi: [10.1093/mnras/stx016](https://doi.org/10.1093/mnras/stx016)
- Güttler, C., Blum, J., Zsom, A., Ormel, C. W., & Dullemond, C. P. 2010, *A&A*, 513, A56, doi: [10.1051/0004-6361/200912852](https://doi.org/10.1051/0004-6361/200912852)
- Hartlep, T., & Cuzzi, J. N. 2020, *ApJ*, 892, 120, doi: [10.3847/1538-4357/ab76c3](https://doi.org/10.3847/1538-4357/ab76c3)
- Hartmann, L., Calvet, N., Gullbring, E., & D'Alessio, P. 1998, *ApJ*, 495, 385, doi: [10.1086/305277](https://doi.org/10.1086/305277)
- Homma, K., & Nakamoto, T. 2018, *ApJ*, 868, 118, doi: [10.3847/1538-4357/aae0fb](https://doi.org/10.3847/1538-4357/aae0fb)
- Homma, K. A., Okuzumi, S., Nakamoto, T., & Ueda, Y. 2019, *ApJ*, 877, 128, doi: [10.3847/1538-4357/ab1de0](https://doi.org/10.3847/1538-4357/ab1de0)
- Jacquet, E., Pignatale, F. C., Chaussidon, M., & Charnoz, S. 2019, *ApJ*, 884, 32, doi: [10.3847/1538-4357/ab38c1](https://doi.org/10.3847/1538-4357/ab38c1)
- Joswiak, D. J., Brownlee, D. E., Matrajt, G., et al. 2012, *M&PS*, 47, 471, doi: [10.1111/j.1945-5100.2012.01337.x](https://doi.org/10.1111/j.1945-5100.2012.01337.x)
- Kataoka, A., Tanaka, H., Okuzumi, S., & Wada, K. 2013, *A&A*, 554, A4, doi: [10.1051/0004-6361/201321325](https://doi.org/10.1051/0004-6361/201321325)
- Kita, N. T., & Ushikubo, T. 2012, *M&PS*, 47, 1108, doi: [10.1111/j.1945-5100.2011.01264.x](https://doi.org/10.1111/j.1945-5100.2011.01264.x)
- Kita, N. T., Yin, Q.-Z., MacPherson, G. J., et al. 2013, *M&PS*, 48, 1383, doi: [10.1111/maps.12141](https://doi.org/10.1111/maps.12141)
- Krijt, S., Ormel, C. W., Dominik, C., & Tielens, A. G. G. M. 2015, *A&A*, 574, A83, doi: [10.1051/0004-6361/201425222](https://doi.org/10.1051/0004-6361/201425222)
- Krot, A. N., Amelin, Y., Bland, P., et al. 2009, *GeoCoA*, 73, 4963, doi: [10.1016/j.gca.2008.09.039](https://doi.org/10.1016/j.gca.2008.09.039)
- Kruijer, T. S., Burkhardt, C., Budde, G., & Kleine, T. 2017, *Proceedings of the National Academy of Science*, 114, 6712, doi: [10.1073/pnas.1704461114](https://doi.org/10.1073/pnas.1704461114)
- Lambrechts, M., & Johansen, A. 2012, *A&A*, 544, A32, doi: [10.1051/0004-6361/201219127](https://doi.org/10.1051/0004-6361/201219127)
- Lehmann, M., & Lin, M. K. 2022, *A&A*, 658, A156, doi: [10.1051/0004-6361/202142378](https://doi.org/10.1051/0004-6361/202142378)
- Lenz, C. T., Klahr, H., Birnstiel, T., Kretke, K., & Stammer, S. 2020, *A&A*, 640, A61, doi: [10.1051/0004-6361/202037878](https://doi.org/10.1051/0004-6361/202037878)
- Lesur, G., Ercolano, B., Flock, M., et al. 2022, *arXiv e-prints*, arXiv:2203.09821, <https://arxiv.org/abs/2203.09821>
- Li, R., & Youdin, A. N. 2021, *ApJ*, 919, 107, doi: [10.3847/1538-4357/ac0e9f](https://doi.org/10.3847/1538-4357/ac0e9f)
- Lin, D. N. C., & Papaloizou, J. 1979, *MNRAS*, 186, 799, doi: [10.1093/mnras/186.4.799](https://doi.org/10.1093/mnras/186.4.799)
- Lin, M.-K. 2019, *MNRAS*, 485, 5221, doi: [10.1093/mnras/stz701](https://doi.org/10.1093/mnras/stz701)
- Lynden-Bell, D., & Pringle, J. E. 1974, *MNRAS*, 168, 603, doi: [10.1093/mnras/168.3.603](https://doi.org/10.1093/mnras/168.3.603)
- Lyra, W., & Umurhan, O. M. 2019, *PASP*, 131, 072001, doi: [10.1088/1538-3873/aaf5ff](https://doi.org/10.1088/1538-3873/aaf5ff)
- Manger, N., Pfeil, T., & Klahr, H. 2021, *MNRAS*, 508, 5402, doi: [10.1093/mnras/stab2599](https://doi.org/10.1093/mnras/stab2599)
- Marcus, P. S., Pei, S., Jiang, C.-H., & Barranco, J. A. 2016, *ApJ*, 833, 148, doi: [10.3847/1538-4357/833/2/148](https://doi.org/10.3847/1538-4357/833/2/148)
- Marcus, P. S., Pei, S., Jiang, C.-H., & Hassanzadeh, P. 2013, *PhRvL*, 111, 084501, doi: [10.1103/PhysRevLett.111.084501](https://doi.org/10.1103/PhysRevLett.111.084501)
- Marrocchi, Y., Villeneuve, J., Jacquet, E., Piralla, M., & Chaussidon, M. 2019, *Proceedings of the National Academy of Science*, 116, 23461, doi: [10.1073/pnas.1912479116](https://doi.org/10.1073/pnas.1912479116)
- Morbidelli, A., Baillié, K., Batygin, K., et al. 2022, *Nature Astronomy*, 6, 72, doi: [10.1038/s41550-021-01517-7](https://doi.org/10.1038/s41550-021-01517-7)
- Morbidelli, A., Bottke, W. F., Nesvorný, D., & Levison, H. F. 2009, *Icarus*, 204, 558, doi: [10.1016/j.icarus.2009.07.011](https://doi.org/10.1016/j.icarus.2009.07.011)
- Nakagawa, Y., Sekiya, M., & Hayashi, C. 1986, *Icarus*, 67, 375, doi: [10.1016/0019-1035\(86\)90121-1](https://doi.org/10.1016/0019-1035(86)90121-1)
- Nanne, J. A. M., Nimmo, F., Cuzzi, J. N., & Kleine, T. 2019, *Earth and Planetary Science Letters*, 511, 44, doi: [10.1016/j.epsl.2019.01.027](https://doi.org/10.1016/j.epsl.2019.01.027)
- National Academies of Sciences, Engineering, and Medicine. 2022, *Origins, Worlds, Life: A Decadal Strategy for Planetary Science and Astrobiology 2023-2032*.
- Nesvorný, D., Li, R., Youdin, A. N., Simon, J. B., & Grundy, W. M. 2019, *Nature Astronomy*, 3, 808, doi: [10.1038/s41550-019-0806-z](https://doi.org/10.1038/s41550-019-0806-z)
- Okuzumi, S., & Hirose, S. 2012, *ApJL*, 753, L8, doi: [10.1088/2041-8205/753/1/L8](https://doi.org/10.1088/2041-8205/753/1/L8)
- Okuzumi, S., Tanaka, H., Kobayashi, H., & Wada, K. 2012, *ApJ*, 752, 106, doi: [10.1088/0004-637X/752/2/106](https://doi.org/10.1088/0004-637X/752/2/106)
- Ormel, C. W., & Klahr, H. H. 2010, *A&A*, 520, A43, doi: [10.1051/0004-6361/201014903](https://doi.org/10.1051/0004-6361/201014903)
- Paardekooper, S.-J., & Johansen, A. 2018, *SSRv*, 214, 38, doi: [10.1007/s11214-018-0472-y](https://doi.org/10.1007/s11214-018-0472-y)
- Paardekooper, S. J., & Mellema, G. 2006, *A&A*, 453, 1129, doi: [10.1051/0004-6361:20054449](https://doi.org/10.1051/0004-6361:20054449)
- Raettig, N., Lyra, W., & Klahr, H. 2021, *ApJ*, 913, 92, doi: [10.3847/1538-4357/abf739](https://doi.org/10.3847/1538-4357/abf739)
- Rice, W. K. M., Armitage, P. J., Wood, K., & Lodato, G. 2006, *MNRAS*, 373, 1619, doi: [10.1111/j.1365-2966.2006.11113.x](https://doi.org/10.1111/j.1365-2966.2006.11113.x)
- Richard, S., Nelson, R. P., & Umurhan, O. M. 2016, *MNRAS*, 456, 3571, doi: [10.1093/mnras/stv2898](https://doi.org/10.1093/mnras/stv2898)
- Schäfer, U., & Johansen, A. 2022, *A&A*, 666, A98, doi: [10.1051/0004-6361/202243655](https://doi.org/10.1051/0004-6361/202243655)

- Schäfer, U., Johansen, A., & Banerjee, R. 2020, *A&A*, 635, A190, doi: [10.1051/0004-6361/201937371](https://doi.org/10.1051/0004-6361/201937371)
- Schoonenberg, D., Ormel, C. W., & Krijt, S. 2018, *A&A*, 620, A134, doi: [10.1051/0004-6361/201834047](https://doi.org/10.1051/0004-6361/201834047)
- Schrader, D. L., Nagashima, K., Krot, A. N., et al. 2017, *GeoCoA*, 201, 275, doi: [10.1016/j.gca.2016.06.023](https://doi.org/10.1016/j.gca.2016.06.023)
- Sekiya, M., & Onishi, I. K. 2018, *ApJ*, 860, 140, doi: [10.3847/1538-4357/aac4a7](https://doi.org/10.3847/1538-4357/aac4a7)
- Sengupta, D., Estrada, P. R., Cuzzi, J. N., & Humayun, M. 2022, *ApJ*, 932, 82, doi: [10.3847/1538-4357/ac6dcc](https://doi.org/10.3847/1538-4357/ac6dcc)
- Sengupta, D., & Umurhan, O. M. 2023, *ApJ*, 942, 74, doi: [10.3847/1538-4357/ac9411](https://doi.org/10.3847/1538-4357/ac9411)
- Simon, J. B., Armitage, P. J., Youdin, A. N., & Li, R. 2017, *ApJL*, 847, L12, doi: [10.3847/2041-8213/aa8c79](https://doi.org/10.3847/2041-8213/aa8c79)
- Simon, J. I., Ross, D. K., Nguyen, A. N., Simon, S. B., & Messenger, S. 2019, *ApJL*, 884, L29, doi: [10.3847/2041-8213/ab43e4](https://doi.org/10.3847/2041-8213/ab43e4)
- Squire, J., & Hopkins, P. F. 2018a, *MNRAS*, 477, 5011, doi: [10.1093/mnras/sty854](https://doi.org/10.1093/mnras/sty854)
- . 2018b, *ApJL*, 856, L15, doi: [10.3847/2041-8213/aab54d](https://doi.org/10.3847/2041-8213/aab54d)
- Stoll, M. H. R., Kley, W., & Picogna, G. 2017, *A&A*, 599, L6, doi: [10.1051/0004-6361/201630226](https://doi.org/10.1051/0004-6361/201630226)
- Suyama, T., Wada, K., Tanaka, H., & Okuzumi, S. 2012, *ApJ*, 753, 115, doi: [10.1088/0004-637X/753/2/115](https://doi.org/10.1088/0004-637X/753/2/115)
- Teague, R., Guilloteau, S., Semenov, D., et al. 2016, *A&A*, 592, A49, doi: [10.1051/0004-6361/201628550](https://doi.org/10.1051/0004-6361/201628550)
- Turner, N. J., Fromang, S., Gammie, C., et al. 2014, in *Protostars and Planets VI*, ed. H. Beuther, R. S. Klessen, C. P. Dullemond, & T. Henning, 411, doi: [10.2458/azu_uapress.9780816531240-ch018](https://doi.org/10.2458/azu_uapress.9780816531240-ch018)
- Umurhan, O. M., Estrada, P. R., & Cuzzi, J. N. 2020, *ApJ*, 895, 4, doi: [10.3847/1538-4357/ab899d](https://doi.org/10.3847/1538-4357/ab899d)
- Umurhan, O. M., Nelson, R. P., & Gressel, O. 2016, *A&A*, 586, A33, doi: [10.1051/0004-6361/201526494](https://doi.org/10.1051/0004-6361/201526494)
- Urpin, V. 2003, *A&A*, 404, 397, doi: [10.1051/0004-6361:20030513](https://doi.org/10.1051/0004-6361:20030513)
- Yang, C.-C., Johansen, A., & Carrera, D. 2017, *A&A*, 606, A80, doi: [10.1051/0004-6361/201630106](https://doi.org/10.1051/0004-6361/201630106)
- Yellin-Bergovoy, R., Heifetz, E., & Umurhan, O. M. 2021, arXiv e-prints, arXiv:2106.04617, <https://arxiv.org/abs/2106.04617>
- Youdin, A. N., & Goodman, J. 2005, *ApJ*, 620, 459, doi: [10.1086/426895](https://doi.org/10.1086/426895)
- Zanda, B., Lewin, E., & Humayun, M. 2018, in *Chondrules: Records of Protoplanetary Disk Processes*, ed. S. S. Russell, J. Connolly, Harold C., & A. N. Krot, 122–150, doi: [10.1017/9781108284073.005](https://doi.org/10.1017/9781108284073.005)
- Zolensky, M. E., Zega, T. J., Yano, H., et al. 2006, *Science*, 314, 1735, doi: [10.1126/science.1135842](https://doi.org/10.1126/science.1135842)
- Zsom, A., Ormel, C. W., Güttler, C., Blum, J., & Dullemond, C. P. 2010, *A&A*, 513, A57, doi: [10.1051/0004-6361/200912976](https://doi.org/10.1051/0004-6361/200912976)